



ELSEVIER

Available online at www.sciencedirect.com

SCIENCE @ DIRECT®

Earth and Planetary Science Letters 227 (2004) 169–177

EPSL

www.elsevier.com/locate/epsl

Ground warming patterns in the Northern Hemisphere during the last five centuries

Hugo Beltrami*, Evelise Bourlon

Environmental Sciences Research Centre and Environmental Earth Sciences Laboratory, St. Francis Xavier University, Antigonish, Nova Scotia, B2G 2W5, Canada

Received 4 March 2004; received in revised form 28 July 2004; accepted 4 September 2004

Available online 18 October 2004

Editor: V. Courtillot

Abstract

Changes in the Earth's surface energy balance recorded underground were used to reconstruct the temperature of the ground surface for the last 500 years in the Northern Hemisphere. We reconstructed ground surface temperature histories (GSTHs) from temperature versus depth profiles measured at 558 sites distributed between 30° and 60°N in the Northern Hemisphere. We show that the ground has warmed about 0.5 K in the last 100 years. Spatial analysis reveals that spatial variability is important and that the weighted average Northern Hemisphere GSTH shows some consistency with multiproxy and meteorological records reconstructions for the last two centuries.

© 2004 Elsevier B.V. All rights reserved.

Keywords: ground temperature; borehole temperatures; ground warming; inversion

1. Introduction

There has been considerable work in borehole climatology in recent times [1–10]. However, the inference of spatial surface energy variations, from these data, has until recently remained unexplored, and spatial analysis using borehole temperature data exist only for Canada [11,12]. In this note, we report on the spatial analysis carried out for data from the Interna-

tional Heat Flow Commission data set, for a mid-latitude sector of the Northern Hemisphere (30–60°N). The data set used in this work contains 105 additional temperature logs that the data set used in [6]. We use a singular value decomposition (SVD) inversion, because the flexibility of this method allows for the separation of the climatic signal into principal components and subsequent reconstructions can be optimized for stability and resolution [13]. Furthermore, SVD selects the components of the ground surface temperature history (GSTH) best represented in the underground signal. This method provides also a safeguard avoiding overparameterization of the GSTH from the inversion [14,15]. We find a consistent increase of the

* Corresponding author. Tel.: +1 902 867 2326; fax: +1 902 867 2457.

E-mail addresses: hugo@stfx.ca (H. Beltrami), ebourlon@stfx.ca (E. Bourlon).

ground surface temperature (GST) over most of the Northern Hemisphere for the period from 1930 to 1980, although the magnitude of the ground energy gained is not spatially homogeneous.

2. Theory

Let us consider the Earth's crust in thermal equilibrium. A temperature–depth profile starts at the surface at the mean-annual ground temperature and increases steadily with depth. If the temperature at the upper boundary of the body is increased, additional heat propagates into the body causing a corresponding increase in temperature just below the surface. The depth to which equilibrium temperatures are perturbed in a given time is governed by the thermal diffusivity of the body. For typical rocks, a thermal front (i.e., 5% change) propagates to about 20 m in 1 year, 50 m in 10 years, 160 m in 100 years, and 500 m in 1000 years. Thus, the Earth's ground temperature history over the last millennium is captured in the uppermost kilometer of the crust. The depth of a temperature perturbation is also related to the timing of surface changes. The shape of the perturbation reveals the details of the surface temperature history. Positive and negative subsurface temperature anomalies are associated with ground surface warming and cooling respectively. Thus, the temperature at depth z , $T(z)$, is the superposition of the quasi-equilibrium temperature and of the temperature perturbation, $T_t(z)$, caused by ground surface temperature variations [16]:

$$T(z) = T_0 + q_0 R(z) + T_t(z) \quad (1)$$

where T_0 is a reference ground temperature, q_0 is the surface heat flow density, $R(z)$ is the thermal depth.

If the past variations of ground surface temperature are modelled as a series of K -step temperature changes, then the subsurface temperature signals from each step change are superimposed, and the temperature perturbation at depth z is given by [14]:

$$T_t(z) = \sum_{k=1}^K T_k \left[\operatorname{erfc} \left(\frac{z}{2\sqrt{\kappa t_k}} \right) - \operatorname{erfc} \left(\frac{z}{2\sqrt{\kappa t_{k-1}}} \right) \right] \quad (2)$$

where T_k are the ground surface temperatures, each value being an average over a period of time $(t_k - t_{k-1})$, erfc is the complementary error function and T_k are the times of the ground surface temperature changes.

The inverse problem consists in determination of T_0 , q_0 and of the ground surface temperature history (GSTH) from $T(z)$. However, T_0 and q_0 could be independently estimated from the upward continuation from the deepest part of the profile, least affected by recent ground surface temperature changes. Eq. (1) is evaluated at every depth where data exist, forming a system of linear equations with $k+2$ unknowns which can be inverted to obtain a series of ground surface temperature values, representing the GSTH at the site.

The system of linear equations can be written as:

$$\Theta_j = \mathbf{A}_{ji} \mathbf{X}_i, \quad (3)$$

where Θ_j is a column vector containing the j -values of temperature measured at depth z_j , \mathbf{X}_i is a column vector containing the model parameters, $i+2$ unknowns (T_0 , q_0 , T_1, \dots, T_k); \mathbf{A}_{ji} is a $(j \times i)$ matrix which contains 1 in the first column, the thermal resistance to depth z_j , $R(z_j)$, in the second column, and the differences between complementary error functions at times t_{k-1} and T_k for depth z_j in columns 3 to $k+2$.

$$\begin{pmatrix} T_1 \\ T_2 \\ \vdots \\ T_j \\ \vdots \\ T_k \end{pmatrix} = \begin{pmatrix} 1 & R_1 & A_{1,3} & A_{1,4} & \dots & A_{1,k+2} \\ 1 & R_2 & A_{2,3} & A_{2,4} & \dots & A_{2,k+2} \\ \vdots & \vdots & \vdots & \vdots & \ddots & \vdots \\ 1 & R_j & A_{j,3} & A_{j,4} & \dots & A_{j,k+2} \end{pmatrix} \begin{pmatrix} T_0 \\ q_0 \\ T_1 \\ \vdots \\ T_k \end{pmatrix}; \quad (4)$$

$$\mathbf{A}_{j,k+2} = \operatorname{erfc} \left(\frac{z_j}{2\sqrt{\kappa t_k}} \right) - \operatorname{erfc} \left(\frac{z_j}{2\sqrt{\kappa t_{k-1}}} \right). \quad (5)$$

The system of linear Eq. (4) can be solved using singular value decomposition (SVD) [17,18,19]. Any matrix $\mathbf{A}(j \times i)$ can be decomposed as $\mathbf{A} = \mathbf{U} \mathbf{\Lambda} \mathbf{V}^T$, where $\mathbf{\Lambda}$ is a $j \times i$ diagonal matrix which contains on the diagonal entries the non-zero singular values $\lambda_{(r)}$ of matrix \mathbf{A} , $r=1, \dots, R$, R is the rank of \mathbf{A} ; $\lambda_{(r)}$ are obtained by square roots of the eigenvalues of the symmetric matrix $\mathbf{A}^T \mathbf{A}$; \mathbf{U} is a $j \times j$ column orthogonal matrix, each column forming a vector, and all j

normed vectors (\mathbf{u}_j) forming a basis into the data space; \mathbf{V} is an $i \times i$ orthogonal matrix, each column forming a vector, and all i normed vectors (\mathbf{v}_i) forming a basis into the model space. The vectors \mathbf{v}_i are also eigenvectors corresponding to the eigenvalues of $\mathbf{A}^T \mathbf{A}$. The eigenvectors that span the model space, \mathbf{v}_i , could be interpreted as the effect on the subsurface of a GSTH given by the eigenvectors that span the data space, \mathbf{u}_j [20].

A general solution is given by [17]:

$$\mathbf{X} = \mathbf{V} \mathbf{\Lambda}^{-1} \mathbf{U}^T \mathbf{\Theta}. \quad (6)$$

Determination of model parameters requires dividing the data by the singular values. Any error in the data will be amplified for the very small singular values. In order to reduce the impact of noise, the singular values which are smaller than a cutoff value are eliminated [21]. Although this is no longer the true solution, SVD selects the linear combination of model parameters that is best constrained by the data. The largest contribution to the standard error in the estimated model parameters is that of the principal component in \mathbf{V} associated with the smallest retained eigenvalue. The variance of the estimated model parameters can be written as [18]

$$\sigma_m^2 = \sum_{r=1}^R \frac{\mathbf{V}_{rm}^2}{\lambda_r^2}. \quad (7)$$

The variance represents the amplification of the measurement errors in the solution (that is, it is the standard error on the estimated parameter corresponding to a 1 K standard deviation in the temperature measurements). As a result of the smoothing performed to allow a proper spatial analysis, the noisiest temperature log included in the analysis is the one determining the resolution retrieved from the data [22]. Individual temperature–depth profile inversion yields results with much more detail. The magnitude of the noise in each borehole temperature profile is the limit of the resolution for a given GSTH. However, since each temperature log was measured by different research teams at different times, each temperature depth profile has a different noise level due to instrumentation sensitivity, stratigraphic noise due to variations of the thermal properties of the underlying rocks. Low noise levels may allow for additional principal components to be

included in the analysis and thus improving the resolution. Higher noise restricts the number of retained principal components and thus reduces the resolution of the retrieved climatic signal. Since this different filtering yields GSTH with different resolutions, it is not possible to individually invert each temperature–depth profile to achieve maximum individual resolution and then attempt to infer common large scale ground temperature changes.

The solutions obtained by retaining only a few singular values, and thus few principal components, can reproduce the gross features of a GSTH [19] and are stable against the presence of data noise. Over-parameterizations, that is, attempts to resolve model parameters of short duration (≤ 20 years), yield unstable solutions without physical meaning. Details of the SVD inversion and its robustness can be found in Refs. [13,14].

3. Analysis

3.1. Inversion

The model for each individual SVD inversion consists of a series of equal duration steps. Fifty-year model step changes in ground surface temperature were used for the last 500 years. The value of the thermal diffusivity was set at $10^{-6} \text{ m}^2 \text{ s}$ [8,23]. The eigenvalue cutoff was set at 0.3 for each GSTH inversion, keeping five principal components for all of the temperature–depth profiles included in the reconstruction. This is a fundamental point as spatial analysis performed from inversions at different resolution or jointly analyzing temperature–depth profiles of different depths are uncertain [11]. Each SVD inversion extracts from the data the long-term surface temperature, semiequilibrium steady state geothermal heat flow density, and the recent climate induced surface temperature changes. These GST changes are expressed throughout this paper as departures from the long-term mean at each location before 1500. Our geothermal based reconstructions of past surface temperatures assume that there is no significant climate variation in scales longer than 500 years. This is a consequence of the decrease in signal and resolution of distant past climatic events [22], and also of the filtering,

arising from the retention of few principal components, required to stabilize the solution obtained from data with different noise levels [13]. The effects of long period events in the distant past, such as the Pleistocene glaciation, are most important at depth of more than 1 km and in our case, these effects are removed with the steady state geothermal gradient correction.

Fig. 1 displays the distribution of the sites and the maximum depth of the borehole temperature logs analyzed in this study. Because data were acquired in holes of opportunity, the spatial distribution of the sites is uneven. Additionally, temperature logs were taken at different times thus it is necessary to incorporate measurement time difference in the inversion. The analysis here represents the temperature recorded up to 1999, although we have restricted our analysis to 1980. Shallow borehole (≈ 200 – 250 m) distribution, and thus a small time window into the past, are well compensated by deep boreholes in all areas.

3.2. Gridding and hemispheric average

In order to avoid giving too much representation to areas in the Northern Hemisphere containing large number of boreholes (Canada, for example), we used a gridding procedure for display purposes. We first filter the data on a $5^\circ \times 5^\circ$ cell grid. A block average method has been applied to compute a mean location and the L2 norm average Δt value in each cell. This is to suppress redundant data and avoid spatial aliasing. Then a surface gridding algorithm produces a $15'$ gridded data set [24]. This algorithm generates

gridded values $z(x,y)$ from unevenly spaced data (x,y,z) by solving the following equation:

$$\left[(1 - \lambda)(\nabla^2)^2 - \lambda(\nabla^2) \right] z(x,y) = 0, \quad (8)$$

where λ is a tension parameter ranging from 0 to 1, and ∇^2 denotes the Laplacian operator: $\nabla^2 = \partial^2/\partial x^2 + \partial^2/\partial y^2$. $\lambda=0$ leads to the biharmonic differential equation and corresponds to the minimum curvature solution that can have unwanted oscillations and false local extrema. $\lambda=1$ corresponds to an infinite tension, it gives a harmonic solution that cannot have local minima and maxima in the free region. The tension parameter we used ($\lambda=0.25$) yields a near minimal curvature surface. We let edges at 20°S and 70°N of latitude be free. The grid is periodic in 360° of longitude. To account for the shrinking size of the geographical cells towards the poles, the gridding procedure was done on a kilometric grid then transferred to a geographical grid using a sinusoidal projection. This area-preserving projection is given by the transformation

$$\begin{cases} x = (\lambda - \lambda_0)\cos\theta \\ y = \theta \end{cases} \quad (9)$$

where λ_0 is the central meridian, (λ,θ) are the longitudinal and latitudinal coordinates, and (x,y) the kilometric coordinates. When mapping the final grid, we draw only the 5° cells which contain at least one borehole and we mask all the oceanic areas. A continuous and equidistant color table was used. We extract the data between 30°N and 60°N at the very end of the processing to avoid edge effects.

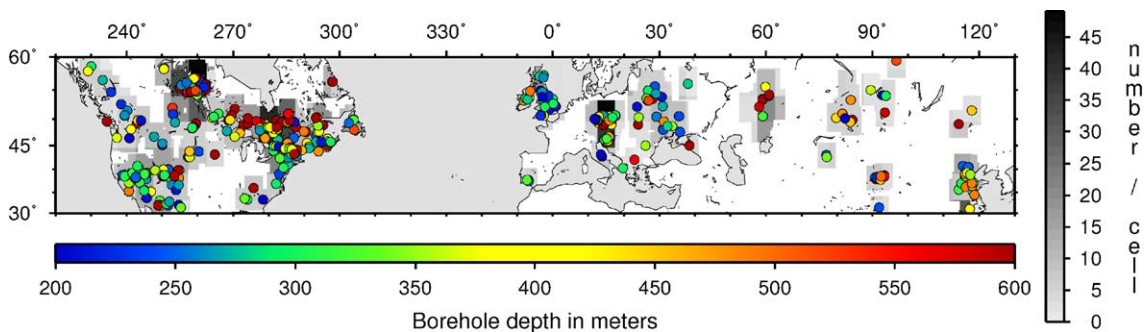


Fig. 1. Borehole density (number of temperature–depth profiles per grid cell), site location, and depth of the borehole temperature logs used in this analysis. Sites are unevenly distributed because measurements are conducted in holes of opportunity.

Because of the sparse spatial distribution of the boreholes, we used an averaging technique to compute the ground surface temperature history rather than a simple arithmetic average. The arithmetic average gives excessive weight to areas of high borehole density. In order to determine hemispheric average, different schemes have already been proposed. Mann et al. [25] argued for an area-weighted average. Pollack and Smerdon [26] have examined this method and another weighting scheme based on grid-cell occupancy. In this paper, we reassess the continental Northern Hemisphere average using a kilometer gridding instead of geographic aggregation. Thus, cells are of the same size and no area weighting is required. Borehole locations were first converted into kilometer units using a sinusoidal projection relative to (0°N, 0°W). Temperature data were averaged on 500×500 km cells to avoid spatial aliasing and suppress redundancy. We did the same for 1000×1000 km cells. These sizes were chosen after several trials to avoid getting too many cells filled with a single borehole, and to have a density as uniform as possible. Grid size effects, however, are not important on the determination of the Northern Hemisphere average [26]. For the 500×500 km case, a total of 154 cells were filled over the world grid. The

occupancy level was at least one borehole, up to 48 with an average of five per grid cell. For the 1000×1000 km case, a total of 84 cells were filled over the world grid. The occupancy level was at least one borehole, up to 29 with an average of seven per grid cell. To avoid that some latitudes (e.g., Canadian latitudes) containing many filled cells distort the hemispheric representation, we give the same weight to all latitudes by filling the empty cells with the average temperature value of their respective latitude. Latitudinal area-weighted average based on 5°×5° and 10°×10° grid cells and a simple arithmetic average was also calculated for comparison purposes.

4. Results and discussion

The resulting averages GSTH from 558 Northern Hemisphere temperature profiles are shown in Fig. 2. The latitudinal area-weighted averages are not significantly different and fall inside the error bar of the latitudinal kilometer averages whatever the cell size considered. The arithmetic average is also shown in Fig. 2 to facilitate comparison with previous works. Our arithmetic average compares well with previous arithmetic average analysis of borehole global data

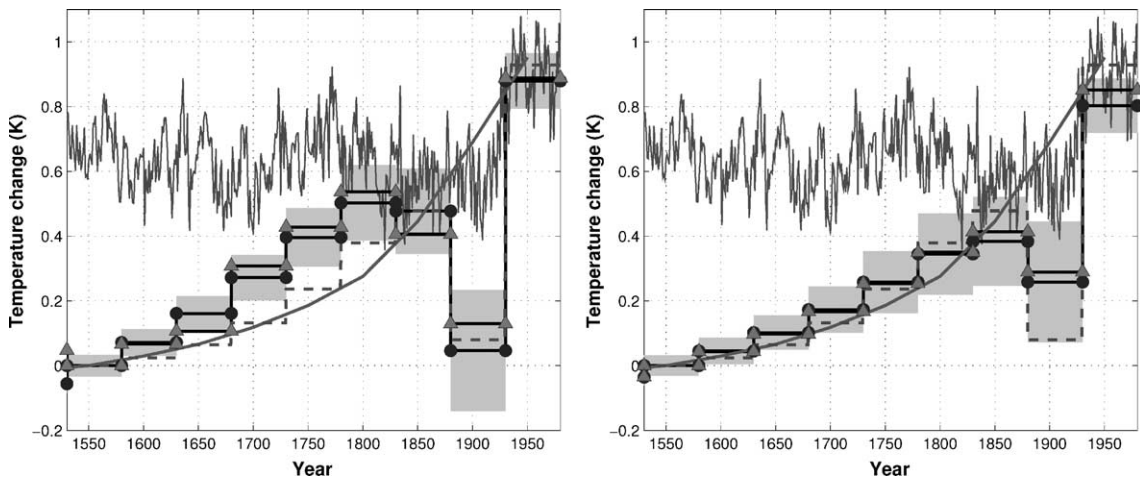


Fig. 2. Average ground surface temperature history for the Northern Hemisphere between 30°N and 60°N from the inversion of 558 temperature–depth profiles. Left panel: Circles represent the latitudinal average based on 500×500 km cell grid. The shaded area represents the stability of the GSTH to the presence of noise in the temperature measurements for this cell size. Triangles represent the latitudinal average based on 5°×5° cell grid. The solid continuous line is Huang et al.'s [6] arithmetic average and the dashed line represents our arithmetic average. Mann et al.'s [37] multiproxy SAT reconstruction are represented by the gray highly variable line. Right panel: Same results but with 1000×1000 km cell gridding (•) and 10°×10° cell grid (△). These different GSTH are presented here to facilitate comparisons. The temperature changes are expressed as departures from the long-term mean (steady-state temperature) at each of the sites analyzed.

[6,8], except for the 50-year colder period from 1880 to 1930 apparent in our results. The average Northern Hemisphere GSTH shows a marked increase in the energy stored in the shallow subsurface since about 1900, consistent with the expectations due to increased levels of greenhouse gases since the onset of the industrial revolution [27]. Average ground temperature increase is about 0.5 K during this period.

Spatial variations of the ground surface temperature are well documented so far only for Canada [12]. Here we examined the spatial distribution of changes in ground surface temperature for the complete continental Northern Hemisphere. Fig. 3 shows the ground temperature changes since 1680 in this area. Clearly, there is a significant ground temperature changes in the recent past. The collection of panels in Fig. 3 shows the series of the spatial distribution of ground temperature variations for several 50-year periods during the last 300 years. The spatial distribution of the recent climatic warming, which appears to be wide spread in some regions shown in Fig. 3, implies that Northern Hemisphere averages must be considered with caution.

It is important to realize that because of heat diffusion, the resolution of borehole temperature data decreases with time [22], such that under the restrictions needed for obtaining robust Northern Hemisphere spatial average, the global inversion cannot retrieve significant information at times before 1500. It is possible to retrieve additional paleoclimatic information from individual borehole inversions. However, since each temperature log has different noise levels, it is often the case that each inversion is performed with a different number of principal components and thus it is extremely difficult to arrive at a common denominator, or GSTHs of equal resolution, to allow for a proper interpretation to obtain an homogeneous global result.

The ground surface temperature since 1500 appears to have been significantly lower than at present. This period includes part of the Little Ice Age cold period reported in some areas of Europe and North America [28,29]. This cold period has been previously detected from individual borehole data inversions in areas of Canada [1,3,12–15,30]. According to Fig. 3, the progression of the warming appears to be South to North, and larger in magnitude in North America than in Eastern Europe. We see no signs of

predominant warming toward the high latitudes, although a more complete analysis incorporating some of the data in the Canadian Arctic is underway, and may provide additional information.

Areas in Central Canada show temporal variations consistent with previous analysis for data in this area [1,4,15]. Labrador and Newfoundland show very little changes with respect to the long-term mean. This is consistent with at least the last 100 years of Environment Canada meteorological data collected in this area of Canada [31], which show a null trend for Newfoundland. Regions in the Mid-West USA (Utah, for example) show little warming in recent years in agreement with meteorological data, and with borehole temperature data from an independent data set not included in our analysis [10].

Cooling is also observed during the 1880–1930 period in regions of North America and Central Europe. This cooling event is however, not synchronous; depending on the averaging method this cooling maybe visible or masked. This period's cooling is reflected in the Northern Hemisphere mean GSTH (Fig. 2) as a decrease in ground surface temperature of about 0.2–0.4 K depending on the averaging technique. This is in agreement with local meteorological records in Romania and Slovenia, and from previous GSTH reconstructions for these areas [32–35]. There is a recovery from these cold anomalies in the second half of the 20th century, with the last 50 years exhibiting an extraordinary energy gain by the ground in agreement with previous studies of heat gain by oceans, atmosphere, cryosphere and continental areas for this time period [7,8,36].

It is not possible to directly compare these results to the analysis carried out by Mann et al. [25,37] for a number of reasons. Mann et al.'s [25] results have been shown to contain errors in the analysis [26] for which a correction has recently appeared in the literature [38]. Furthermore, the analysis performed by Mann et al. [25], compared SAT records at grid sizes too small ($5^{\circ} \times 5^{\circ}$) to be meaningful because of the sparse population of borehole records [26]. We have included the $5^{\circ} \times 5^{\circ}$ Northern Hemisphere average results only to facilitate comparison. Larger grids ($10^{\circ} \times 10^{\circ}$) are needed to increase confidence in the average (see Fig. 2).

A factor that might help explain the disagreement of the multiproxy reconstruction and borehole-based

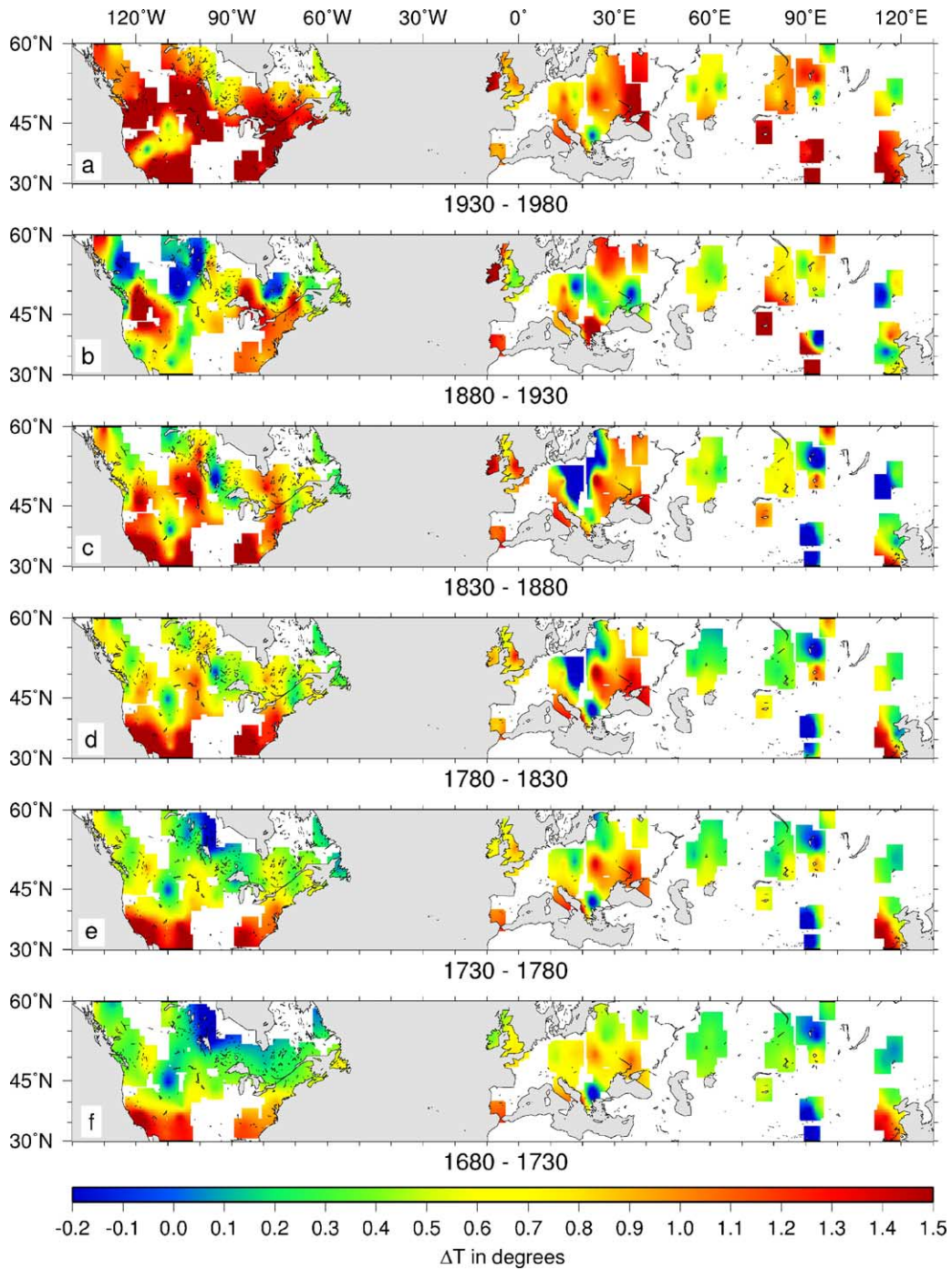


Fig. 3. (a–f) Spatial distribution of the ground surface temperature history for the period between 1680 and 1980. The GSTH are expressed as departures from the long-term mean before 1500 at each location. The results are presented for 50-year time intervals. This figure was constructed from the results of the inversion of 558 temperature depth profiles in the Northern Hemisphere between 30°N and 60°N. All inversions included in the analysis were performed with the same eigenvalue cutoff. The same number of principal components was included in the reconstruction of each GSTH. This is required for performing a spatial analysis at the same resolution to allow for proper comparison.

reconstruction rests in the different sensitivity of these records. The multiproxy reconstruction [37] is strongly based on dendrochronological data which are known not to preserve the long-term trends [39]. This is because each single tree ring series is fitted with a different and arbitrary “growth trend removal” function. Removal of the growth trend filters out long-term variations and removes climatic information from a different frequency band for each tree-ring series before individual series are combined into a site chronology. A recent work [40] has found that long-term trend removal from tree-ring series does in fact explain the discrepancies between geothermal and multiproxy reconstruction. Furthermore, tree-growth records growth season temperature and precipitation, and unlike geothermal data, trees do not integrate the energy balance at the Earth’s surface over the whole year. Ground temperature histories, on the other hand, are long-term indicators of the energy balance at the surface. Thus, the heat budget in the subsurface is a long-term response of the Earth to energy balance changes at its surface.

5. Conclusions

Even if some disagreements on climatic reconstructions from geothermal and multiproxy data exist, our results are encouraging. This study points out some consistency with multiproxy and meteorological records at least for the two last centuries in Central Europe, Mid-West North America, and Eastern Canada. We do not expect an agreement between multiproxy and geothermal data prior to 1800 due to the long-period signal removal during the analysis of dendrochronological data [40]. The cold excursion at the beginning of the last century, not observed in previous works (e.g., Huang et al.’s [6] arithmetic average), is recovered with all area-weighted averaging procedures we used. We observe warming of almost 1 °C for the last five centuries, half of this warming occurred during the last 50 years.

Acknowledgments

This research was funded by the Canadian Foundation for Climate and Atmospheric Sciences (CFCAS)

and the Natural Sciences and Engineering Research Council of Canada (NSERC). Comments by V. Cermák and an anonymous reviewer help us to improve this communication. B. Quinn helped us with the codes at the early stages of this work.

References

- [1] H. Beltrami, A.M. Jessop, J.C. Mareschal, Ground temperature histories in eastern and central Canada from geothermal measurements: evidence of climate change, *Glob. Planet. Change* 98 (1992) 167–183.
- [2] H. Beltrami, J.C. Mareschal, Recent warming in eastern Canada inferred from geothermal measurements, *Geophys. Res. Lett.* 18 (1991) 605–660.
- [3] H. Beltrami, R.N. Harris (Eds.), Inference of Climate Change from Geothermal Data, *Glob. Planet. Change* 29 (2001) 148–352.
- [4] H. Beltrami, On the relationship between ground temperature histories and meteorological records: a report on the Pomquet station, *Glob. Planet. Change* 29 (2001) 327–352.
- [5] H.N. Pollack, S. Huang, Climate reconstructions from subsurface temperatures, *Annu. Rev. Earth Planet. Sci.* 28 (2000) 339–365.
- [6] S. Huang, H.N. Pollack, P.Y. Shen, Temperature trends over the last five centuries reconstructed from borehole temperatures, *Nature* 403 (2000) 756–758.
- [7] H. Beltrami, J. Smerdon, H.N. Pollack, S. Huang, Continental heat gain in the global climate system, *Geophys. Res. Lett.* 29 (2002) DOI:10.1029/2001GL014310.
- [8] H. Beltrami, Climate from borehole data: energy fluxes and temperatures since 1500, *Geophys. Res. Lett.* 29 (23) (2002) 2111.
- [9] H. Beltrami, Earth’s long-term memory, *Science* 297 (2002) 206–207.
- [10] R.N. Harris, D.S. Chapman, Mid latitude (30°–60° N) climatic warming inferred by combining borehole temperature with surface air temperature, *Geophys. Res. Lett.* 28 (2001) 747–750.
- [11] J. Majorowicz, J. Safanda, W. Skinner, East to west retardation in the onset of the recent warming across Canada inferred from inversions of temperature logs, *J. Geophys. Res.* 107 (2002) DOI:10.1029/2001JB000519.
- [12] H. Beltrami, C. Gosselin, J.C. Mareschal, Ground surface temperatures in Canada: spatial and temporal variability, *Geophys. Res. Lett.* 30 (10) (2003) 1499.
- [13] H. Beltrami, L. Cheng, J.C. Mareschal, Simultaneous inversion of borehole temperature data for past climate determination, *Geophys. J. Int.* 129 (1997) 311–318.
- [14] J.C. Mareschal, H. Beltrami, Evidence for recent warming from perturbed geothermal gradients: examples from eastern Canada, *Clim. Dyn.* 6 (1992) 135–143.
- [15] H. Beltrami, J.C. Mareschal, Ground temperature histories for central and eastern Canada from geothermal measure-

- ments: Little Ice Age signature, *Geophys. Res. Lett.* 19 (1992) 689–692.
- [16] H.S. Carslaw, J.C. Jaeger, *Conduction of Heat in Solids*, 2nd ed., Oxford Univ. Press, New York, 1959, 510 pp.
- [17] C. Lanczos, *Linear Differential Operators*, D. Van Nostrand, New York, 1961, 564 pp.
- [18] D.D. Jackson, Interpretation of inaccurate, insufficient, and inconsistent data, *Geophys. J. R. Astron. Soc.* 28 (1972) 97–110.
- [19] W. Menke, *Geophysical Data Analysis: Discrete Inverse Theory*, Int. Geophys. Ser., vol. 45, Academic, San Diego, CA, 1989, 289 pp.
- [20] G. Vasseur, Ph. Bernard, J. Van De Meulebrouck, Y. Kast, J. Jolivet, Holocene paleotemperatures deduced from geothermal measurements, *Palaeogeogr. Palaeoclimatol. Palaeoecol.* 43 (1983) 237–259.
- [21] R.A. Wiggins, The general linear inverse problem: implication of surface waves and free oscillations for Earth structure, *Rev. Geophys.* 10 (1972) 251–285.
- [22] H. Beltrami, J.C. Mareschal, Resolution of ground temperature histories inverted from borehole temperature data, *Glob. Planet. Change* 11 (1995) 57–70.
- [23] V. Čermák, L. Rybach, Thermal conductivity and specific heat of minerals and rocks, in *Landolt-Bornstein; Zahlenwerte und Funktionen aus Naturwissenschaften und Technik*, in: G. Angenheister (Ed.), (Hrsg.) Bd. 1, Physikalische Eigenschaften der Gesteine, Teilbd. a, Springer-Verlag Berlin, Heidelberg, 1982, pp. 305–343.
- [24] W.H.F. Smith, P. Wessel, Gridding with continuous curvature splines in tension, *Geophysics* 55 (1990) 293–305.
- [25] M.E. Mann, S. Rutherford, R.S. Bradley, M.K. Hughes, F.T. Keimig, Optimal surface temperature reconstructions using terrestrial borehole data, *J. Geophys. Res.* 108 (D7) (2003) 4203.
- [26] H.N. Pollack, J.E. Smerdon, Borehole climate reconstructions: spatial structure and hemispheric averages, *J. Geophys. Res.* 109 (2004) D11106.
- [27] J.T. Houghton, G.J. Jenkins, J.J. Ephraums (Ed.), *Climate change 2001: the scientific basis: contribution of Working Group I to the third assessment report of the Intergovernmental Panel on Climate Change*. Edited by J.T. Houghton, Y. Ding, D.J. Griggs, M. Noguer, P.J. van der Linden, X. Dai, K. Maskell, and C.A. Johnson (eds.), Cambridge University press, Cambridge, 2001, 881 pp.
- [28] J.M. Grove, The initiation of the “Little Ice Age” in regions round the North Atlantic, *Clim. Change* 48 (2001) 53–81.
- [29] B.H. Luckman, Calendar-dated “Little Ice Age” glacier advance at Robinson Glacier, British Columbia, Canada, *Holocene* 5 (1995) 149–159.
- [30] T. Lewis (Ed.), *Climatic Change Inferred from Underground Temperatures*, *Glob. Planet. Change* 98 (1992) 78–282.
- [31] D.W. Gullett, W.R. Skinner, The state of Canada’s climate: temperature change in Canada 1895–1991, *Environ. Rep.*, vol. 92-2, Environ. Canada, Ottawa, 1992.
- [32] D. Rajver, J. Šafanda, P.Y. Shen, The climatic record inverted from borehole temperatures in Slovenia, *Tectonophysics* 291 (1998) 263–276.
- [33] B. Župančič, Mean annual temperature for Ljubljana, Unpubl. data, Hydrometeorological Survey of Slovenia, Ljubljana, 1994.
- [34] L. Bodri, V. Cermak, Last 250 years climate reconstruction inferred from geothermal measurements in the Czech Republic, *Tectonophysics* 291 (1998) 251–261.
- [35] C. Clauser, J.C. Mareschal, Ground temperature history in Central Europe from borehole temperature data, *Geophys. J. Int.* 121 (1995) 805–817.
- [36] S. Levitus, J. Antonov, J. Wang, T.L. Delworth, K. Dixon, A. Broccoli, Anthropogenic warming of the Earth’s climate system, *Science* 292 (2001) 267–270.
- [37] M.E. Mann, R.S. Bradley, M.K. Hughes, Northern Hemisphere temperatures during the past millennium: inferences, uncertainties, and limitations, *Geophys. Res. Lett.* 26 (1999) 759–762.
- [38] S. Rutherford, M.E. Mann, Correction to “Optimal surface temperature reconstructions using terrestrial borehole data”, *J. Geophys. Res.* 109 (2004) D11107.
- [39] J. Esper, E.R. Cook, F.H. Schweingruberg, Low-frequency signals in long tree-ring chronologies for reconstructing past temperature variability, *Science* 295 (2002) 2250–2253.
- [40] J. Esper, D.C. Frank, R.J.S. Wilson, Climate reconstructions: low-frequency ambition and high-frequency ratification, *EOS* 85 (12) (2004) 113–120.